R. C. Sampson
2 June 1972

PHOTOELASTIC STRESS ANALYSIS METHODOLOGY AND APPLICATIONS TO NERVA STRUCTURES

I. INTRODUCTION

Photoelasticity is a well-recognized and continually developing technique for experimental stress analysis. It is unique among all experimental and numerical methods in regard to the complexity of the structural geometry that can be solved exactly. Similarly, its high resolution capability for analysis of rapid spatial variations of stress is unrivaled by any other experimental technique. In spite of this technical superiority in these areas, photoelasticity is not routinely applied for purposes of stress analysis. It finds best application to specially selected problems, and the reasons for this are clear. The demand for increasingly sophisticated stress analysis in recent years has been paralleled by developments in computer technology and numerical methods for stress analysis. In a great many instances the numerical "model" is of at least equal validity to the photoelastic model. Equally important, numerical modeling often lends itself better to rapid and economical production of data since engineering personnel customarily receive education that equips them for more readily absorbing the numerical rather than the experimental techniques. And, since numerical methods involve mathematical abstractions rather than physical quantities, delays and inertia in making changes in the "model" or its testing sequence are often correspondingly less. Consequently, numerical stress work schedules may be more reliably achieved, at least in principle.

In view of the foregoing, it is not remarkable that stress analysis relies to a very great extent upon numerical techniques. Photoelasticity retains at

(NASA-CR-132213) PHOTOELASTIC STRESS ANALYSIS METHODOLOGY AND APPLICATIONS TO NERVA STRUCTURES (Aerojet-General Corp., Sacramento, Calif.) 35 37 p HC $3.75
CSCL 21F G3/22
N73-24673
Unclas 17731

least four important functions in industrial stress analysis, however. These are: (a) analysis of three-dimensional structures too complex to be modeled numerically within the limitations of the available programs and machines, (b) the experimental verification of stress predictions obtained from new, untried computer programs, (c) modeling structures which are composed of two or more contacting components and in which the contact boundary conditions change with increased loading, and (d) verification of approximate methods for solving three-dimensional stress problems by utilizing two-dimensional numerical techniques. Examples where these functions have led to the employment of photoelastic techniques are plentiful in the literature. Appendix A contains some examples of these and other applications. Other examples are provided by References [1]* through [3], and Reference [12].

Three major applications of photoelasticity were made to NERVA structures components during the course of the program. A review of this experimental work and some of the benefits derived from it is contained in a later section of this report.

II. OUTLINE OF PHOTOELASTICITY PRINCIPLES

A. THEORY

In this brief outline, attention will be directed to the transparent plastic model materials that possess isotropic elasticity and which exhibit temporary double refraction under stress [4],

$$R = Ct\ (\sigma_1 - \sigma_2) \tag{1}$$

---

*Reference numbers are in square brackets throughout this report.

where R = the relative retardation of transmitted light

C = the material stress-optic coefficient

t = model thickness

$(\sigma_1 - \sigma_2)$ = the difference of the major and minor principal stresses

This relation is depicted graphically at the top of Figure (1) where a plane stressed cubical element is shown being traversed by a single ray of polarized light that has been resolved into in-phase components in the two planes of principal stress. Below, the simplest of all polariscope configurations is depicted, consisting of a crossed polarizer and an analyzer. The function of each element is described there. This polariscope provides not only the relative retardation caused by stress, but also direction, θ, of the principal stress with respect to the x-axis.

A plane stressed cubical element oriented to the x, y coordinate system is subjected to the normal stress components σ_{xx} and σ_{yy}, and shear stress τ_{xy}. The principal stresses are related to these stress components by the static equilibrium requirements:

$$\sigma_1 = \frac{\sigma_{xx} + \sigma_{yy}}{2} + \frac{1}{2}\sqrt{\frac{\sigma_{xx} - \sigma_{yy}}{2}^2 + 4\tau_{xy}^2} \qquad (2)$$

$$\sigma_2 = \frac{\sigma_{xx} + \sigma_{yy}}{2} - \frac{1}{2}\sqrt{\frac{\sigma_{xx} - \sigma_{yy}}{2}^2 + 4\tau_{xy}^2} \qquad (3)$$

and $$\theta = \frac{1}{2}\tan^{-1}\frac{2\tau_{xy}}{(\sigma_x - \sigma_y)} \qquad (4)$$

The inverse relations are:

$$\sigma_x = \sigma_1 \cos^2\theta + \sigma_2 \sin^2\theta \tag{5}$$

$$\sigma_y = \sigma_1 \sin^2\theta + \sigma_2 \cos^2\theta \tag{6}$$

$$\tau_{xy} = \frac{\sigma_1 - \sigma_2}{2} \sin 2\theta \tag{7}$$

The retardation R depicted in Figure 1 is the stress-induced spatial phase lag introduced in the plastic model by the difference of the principal stresses. Its physical origin is in the change of the refractive index accompanying changes of stress in such plastics. Thus the velocity of the light ray component polarized in the σ_1 plane is not the same as that of the other component beam polarized in the σ_2 plane. The beams enter the element in phase but emerge out of phase. In terms of the engineering quantities generally employed in photoelastic analysis, equation (1) becomes

$$n = \frac{(\sigma_1 - \sigma_2)t}{f} \tag{8}$$

where n = retardation in units of multiples of the wave length of the monochromatic light employed, fringe order*

f = the "stress-fringe value", a material constant, psi-inches per fringe

*The term "birefringence" is commonly used to denote the occurrence of this double refraction phenomenon. Thus, n is the amount of birefringence.

Knowing the model thickness, the fringe order and the stress-fringe value it is seen that one may readily solve for the difference of principal stress at any point in the photoelastic model.

Equation (8) is sufficient to determine the surface stress tangent to the model or slice edge, when that surface is free of contact with another solid body. In order to determine the true principal stresses, which are not necessarily coincident with the slice plane, supplementary methods must be employed. Chief among these are the method of oblique incidence and the method of sub-slicing for frozen-stressed models. [5]

Interior stress (stress at other than boundary locations, or at boundary locations where contact with another solid occurs) are also investigated. The "shear-difference" method [6] offers the most practical approach for "frozen-stress" experiments, though the oblique incidence approach is also useful, in principle.

B. MODEL/PROTOTYPE RELATIONS

Stresses and deflections determined from the subscale photoelastic model are ultimately interpreted in terms of the full scale prototype. Model-prototype scaling laws emerge from dimensional analysis procedures and from consideration of the laws which govern similitude between the model and the prototype, [7]. These laws can be readily deduced for the simplest case of an externally loaded, rigid, elastic structure which behaves in a linear manner. The stress in a solid body which fits this description can be expressed functionally as

$$\sigma = \frac{P}{a^2} \cdot F_\sigma \left(\frac{x}{a}, \frac{y}{a}, \frac{z}{a}, \nu, S\right) \qquad (9)$$

where P = the applied force vector

a = a characteristic dimension of the body

x, y, z = the coordinate position of the stressed point

ν = Poisson's ratio, a material constant

S = a complete definition of the shape of the body.

If the stress is put in dimensionless form,

$$\frac{\sigma a^2}{P} = F_\sigma \left(\frac{x}{a}, \frac{y}{a}, \frac{z}{a}, \nu, S\right) \quad , \tag{10}$$

the dimensionless stress is seen to be a function only of those parameters within the brackets. If each of these parameters is the same for the model as for the prototype, then their dimensionless stress at corresponding points will also be the same. Similar reasoning also applies to more complex conditions.

By the same reasoning as above, the dimensionless deflections of either the model or the prototype are given by

$$\frac{Ea\delta}{P} = F_\delta \left(\frac{x}{a}, \frac{y}{a}, \frac{z}{a}, \nu, S\right) \tag{11}$$

Again the terms within the brackets on the right hand side must be identical in both the model and the prototype in order that exact predictions of prototype deflection may be made from observations of the model deflection. The effect of differences in these parameters varies considerably. Each case should be evaluated separately rather than relying on generalizations.

The behavior of the viscoelastic materials employed in photoelasticity becomes very complex under certain circumstances. Nearly all photoelastic testing is conducted at temperatures where the physical and optical

behavior of the material is essentially independent of time. Interpretation of the "stress patterns" is thus greatly simplified. An outline of photoelastic materials behavior follows.

C. MATERIALS BEHAVIOR

A typical photoelastic material is characterized schematically with regard to birefringence (or strain) as a function of temperature and time in the manner illustrated in Figure (2). Briefly, there are two regions of this "contour map" where the photoelastic response of the material is, for all practical purposes, independent of time and/or small changes of temperature. These regions are those labeled "Rubbery" and "Glassy". A photoelastic material of great practical value for plane stress modeling must have a glassy region that extends well above ordinary room temperature. Materials useful for three-dimensional "frozen-stress" analysis must have their rubbery regions occurring at temperatures low enough that surface oxidation or other thermally activated chemical changes do not occur to a significant degree. For most purposes, the "Transition" region in Figure (2) is not specifically utilized in photoelastic testing, though exceptions have been noted in very special investigations [8].

The "freezing of stress" is of special importance in photo-elasticity because it enables the permanent fixing of the stress-induced birefringence system in a three-dimensional structure. Loading fixtures are removed and the model dissected at leisure for examination of all the stressed locations of interest. In order to better describe this process, a schematic representation of the photoelastic material as an arrangement of springs and dashpots is helpful, Figure (3). This "model" is consistent with the behavior represented in Figure (2), when the model elements are as defined in the legend of Figure (3). Briefly

stated, if a constant stress is applied to the material for a sufficiently long time, the birefringence will reach a value n_{max} where no further increases with time will be noted, independent of temperature. However, if the material is first heated to its "critical" temperature, T_{cr}, it will achieve the value n_{max} almost instantly and maintain that value indefinitely so long as the stress and temperature are maintained constant. At that elevated temperature, the dashpot viscosities η_1 and η_2 tend toward zero and the elastic elements that predominate at room temperature, K_1, and K_2, no longer sustain any load. All the birefringence and strain is accumulated in the relatively soft "spring" K_3. It must be recalled, however, that while Figure (3) is a functional model that behaves in the same general manner as the photoelastic material, the actual mechanisms involved in these polymeric materials are far more complex. For that reason, functional models like that in Figure (3) are completely inadequate for quantitative characterization of actual materials. Nevertheless, employing this model helps to understand the general behavior, if not the true origins, of photoelastic testing principles. For example the distinction between the behavior of cross linked and uncrosslinked polymers is depicted in Figure (4), the difference being in the values prescribed for the steady flow dashpot η_3 in Figure (3). The various stages of deformation, where different model elements predominate, are indicated by letter-designated segments on the curves of Figure (4). At time t_1, the load was removed in this illustration, and it is seen that the uncrosslinked material experiences a permanent set, whereas the crosslinked material "remembers" its original stress free state after a period of time.

"Stress freezing" materials are of the crosslinked type. The photoelastic behavior of a typical material during the process of stress freezing is

shown schematically in Figure (5). For simplicity, the behavior of a uniaxial tensile specimen is represented there. No essential difference of behavior is introduced regardless of the geometric complexity of the structural model. The significant stages of the process are labeled on the curve in Figure (5), with letters designating the terminals of each phase. It is seen that the process consists sequentially of a loading phase, a heating phase, a cooling phase and an unloading phase. The sequence of corresponding events in the functional model, Figure (3), can be readily appreciated. The final condition is one where spring element K_3 is held in an extended condition by the relatively very rigid spring elements K_2 and K_3. Elastic energy of deformation is thus stored within the system, and in the actual material this storage takes place on the molecular scale. Thus, the cutting or destruction of a part of the model has no effect on those remaining elements only a few molecular crosslinks distant from the cut.

In the manner just described schematically, the total stress system is permanently stored in three-dimensional structural models. Almost unlimited dissection of the model is permissible, since no significant release of stored energy occurs in the remaining material. Analysis may be initiated immediately or at any finite later time, and it may be as cursory or as detailed as the investigator wishes. It is not surprising therefore that the "frozen stress" photoelastic technique finds far more practical application than any other method in photoelasticity.

III. APPLICATIONS TO NERVA STRUCTURES PROBLEMS

Three photoelastic investigations were conducted in the course of the NERVA program. These three are listed in chronological order as References [9], [10], and [11]. An outline of each, stating the problem and the principal test results, follows.

A. ROLLER BEARING, Reference [9]

The roller bearing, Figure (6), was required to operate with the loose-fitting shaft axis misaligned as much as 0° - 30' with the bearing axis, and an unfavorable localization of load occurred on the rollers. Failures of the inner race were experienced in test operations. Photoelastic model tests were undertaken for the purpose of determining the location and magnitude of peak stresses. Two model tests were conducted, Test I with the cylindrical rollers having standard corner relief and Test II with a generous radius corner relief. The photoelastic plastic models were tested by the "frozen stress" technique in which the structurally similar model was statically loaded with appropriately scaled dead weights in an oven which was heated to the critical temperature, T_{cr}. For the material employed in these tests, HYSOL 4390, the critical temperature was 128°C. The proper inclination of the shaft was regulated and controlled by adjusting the position of the weight hangars, Figure (7).

Numerous slices were removed from the models after completion of the tests. Slices taken from two corresponding rollers in the two tests are shown in Figure (8). The stress distributions were charted at a number of locations on the inner race and converted to stress in the prototype by appropriate similarity relations, equation (10). A comparison of the inner race meridional stress distribution for Test I (Figure (9)) and Test II (Figure (10)) is shown.

The experimental results showed that major differences in contact surface stress existed in the standard and the modified roller when shaft misalignment was introduced. Modification of the bearing roller ends as in model Test II was concluded to offer significant improvements in the bearing stress concentration.

B. BUTTERFLY VALVE LIP SEAL (P/N 1117995-11), Reference [10]

Three-dimensional photoelastic models were employed to determine separately the elastic stress distribution caused by seating forces and by pressurization forces. The lip seal gate valve prototypes provide flow control in a liquid hydrogen supply line. The rotating gate wipes against the edge of the lip-seal ring in closing, enforcing a certain radial displacement of the ring. When the gate valve is opened, a substantial fluid pressure differential is momentarily established across the seal ring. The photoelastic model test fixtures were designed to model, by static testing means, these two separate loading conditions.

The valve seating load test setup is shown in cross-section on Figure (11) and the pressure test setup in Figure (12). In each case, "freezing" of the model stresses was accomplished in the conventional manner, and meridional slices were removed from the seal ring for analysis. Figure (13) shows the photoelastic "frozen-stress" freeze pattern in a representative slice taken from each test.

The analysis of these stress patterns showed that the proposed seating conditions will produce forces in the prototype that will induce lip seal ring stresses well above the yield point. Transient stresses due to the momentary pressure drop across the prototype seal ring, due to valve opening, were found to be below the yield point except very locally near the retaining ring clamp location.

C. IMPELLER ROTOR, Reference [11]

Verification of stress levels in the TPA impeller first stage rotor was required, due to the extreme complexity of the stress analysis problem. The spiral blades of the impeller posed especially severe problems in devising a

suitable finite element model for computation of stresses. Therefore an accurate, full scale photoelastic model, Figure (14), was prepared and installed in a spin-test fixture inside a "stress-freezing" oven, Figure (15). Rotation of the model at a speed of only 1758 rpm was sufficient to induce "frozen" stresses and deflections that enabled a thorough analysis. Projecting the model stresses and deflections in terms of the prototype rotating at much higher speed was later accomplished through model/prototype similarity conditions similar to Equations (10) and (11).

A typical "frozen-stress" slice taken from a meridional plane through one of the blade tips is shown at left in Figure (16). The value of the fringe order n is noted at several places on that photograph. These values were measured at all significant surface stress locations, and the boundary stress determined by Equation (8). In all, 41 slices were removed from various planes and the numerous peak surface stresses determined. Demonstrating the reversible elastic nature of "frozen" stresses, the slice at left in Figure (16) was reheated to its test temperature and slowly cooled. Again viewing it in the polariscope, at right in Figure (16), it is seen that all traces of the spin-induced elastic stress pattern have disappeared.

As a follow-on to this experiment, a finite element computation model was developed [12] which greatly improved the accuracy of stress calculations above that formerly obtained on the basis of finite element models derived from largely intuitive representations. The improved finite element models provided calculated peak stresses that agreed within 10 percent, on the average, with the experimental results, while the maximum stresses in the models agreed within 4 percent. Experimentation with the finite element model also indicated that

Poisson's ratio has a significant effect on the stresses experienced in the impeller, particularly in the blade/shroud region.

IV. —REFERENCES

1. Dally, J. W. and Riley, W. R., "Experimental Stress Analysis", McGraw-Hill Book Company, New York, 1965

2. Leven, M. M. and Sampson, R. C., "Photoelastic Stress and Deformation Analysis of Nuclear Reactor Components", Proceedings of Society for Experimental Stress Analysis (SESA), Vol. XVII, 1959

3. Sampson, R. C. and Campbell, D. M., "Contributions of Photoelasticity to Evaluation of Solid Propellant Motor Integrity", AIAA Journal for Spacecraft and Rockets, April, 1966

4. Frocht, M. M., "Photoelasticity, Vol. I", John Wiley and Sons, New York, 1957, p. 136

5. Leven, M. M., "Quantitative Three-Dimensional Photoelasticity", Proceedings of the SESA, Vol. XII, No. 2, pp. 157-171, 1955

6. Frocht, M. M. and Guernsey, R., Jr., "Studies in Three Dimensional Photoelasticity", Proceedings of 1st U. S. National Congress Applied Mechanics, pp. 301-307, June 1951

7. "Handbook for Experimental Stress Analysis", M. Hetenyi, Editor, John Wiley and Sons

8. Dill, E. H. and Fowlkes, C. W., "Photoviscoelasticity", NASA CR-444, May 1965

9. Sampson, R. C., "Frozen-Stress Photoelastic Analysis of a Roller Bearing", Aerojet-General Corporation Propulsion Division Report PEL-64, May 1968

10. Campbell, D. M., "Three-Dimensional Photoelastic Analysis of a Five-Inch Butterfly Valve Lip-Seal (P/N 1117995)", Aerojet-General Corporation Report PEL-66, November 1968

11. Sampson, R. C. "Frozen Stress Photoelastic Analysis of the TPA First Stage Impeller Model 1139253-1 N/C", ANSC Engineering Operations Report N8120R:71-011, November 1971

12. Sampson, R. C. and McMullen, F. E., "Development of a Computational Model for Optimum Correlation with the Photoelastic Test Data for the First Stage TPA Impeller", ANSC Engineering Operations Report N8120R:72-031, April 1972

FIG. 1 THE PHOTOELASTIC EFFECT

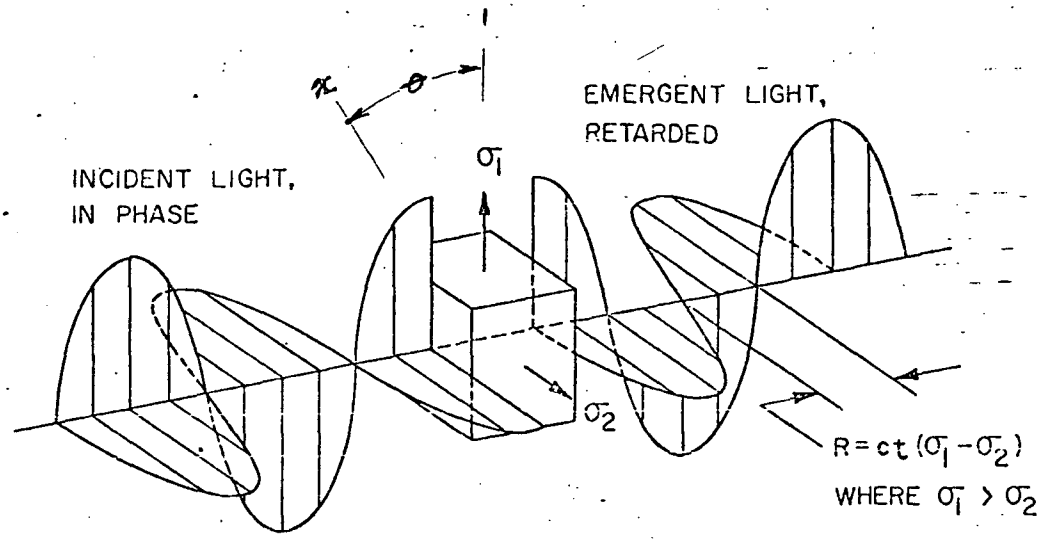

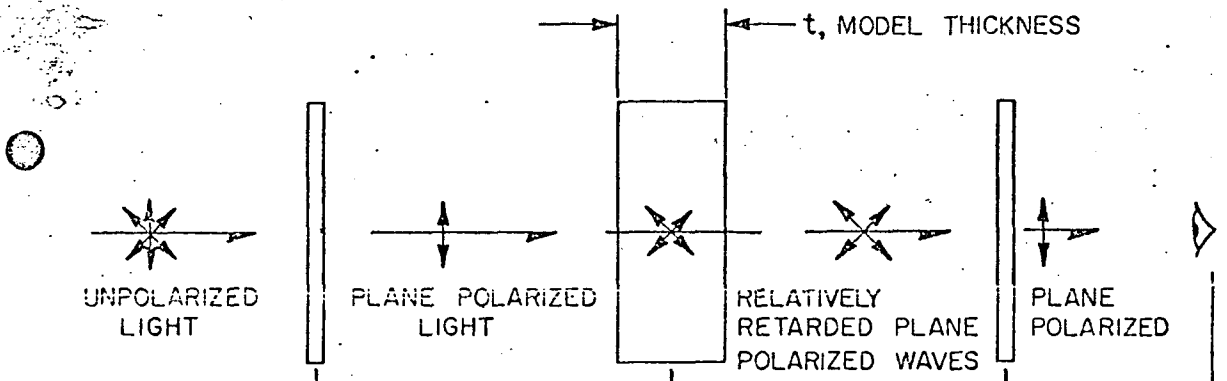

POLARIZER
ELIMINATES LIGHT VIBRATIONS IN ALL BUT ONE PLANE.

MODEL
TRANSMITS PLANE POLARIZED LIGHT ON σ_1 AND σ_2 PLANES. PROGRESSIVELY RETARDS ONE WAVE RELATIVE TO ANOTHER.

ANALYZER
RESOLVES RETARDED WAVES ON ONE PLANE. TRANSMITTED LIGHT INTENSITY VARIES WITH RELATIVE RETARDATION.

OBSERVER
SEES PATTERN OF FRINGES CORRESPONDING TO CONSTANT VALUES OF $(\sigma_1 - \sigma_2)$.

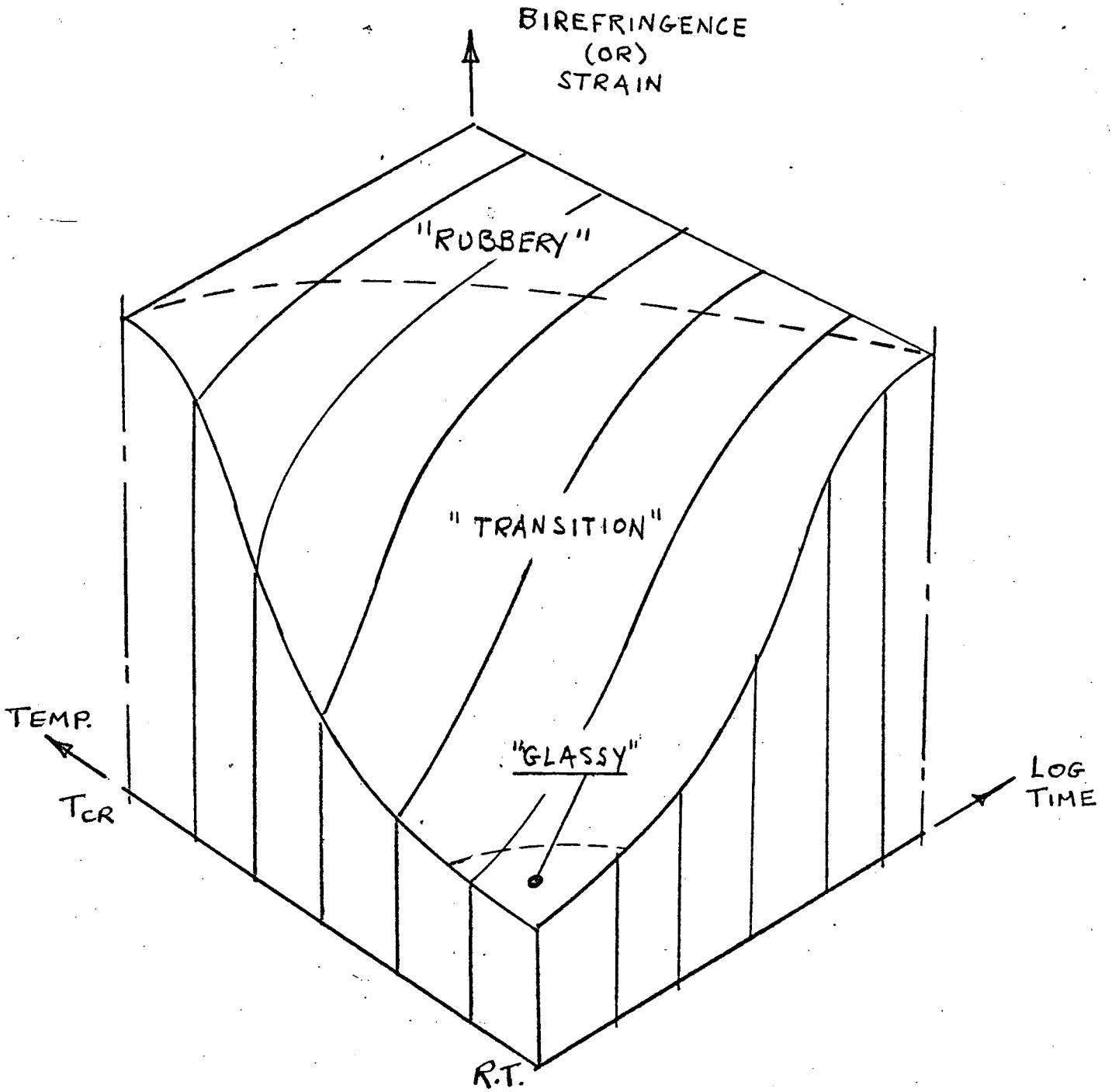

FIG. 2 TIME - TEMPERATURE BEHAVIOR OF PHOTOELASTIC MATERIAL AT CONSTANT STRESS.

LEGEND

K_3 Rubbery Elasticity
η_3 Steady Flow (No Crosslinking)
η_2 Long-Term Viscosity
η_1 Short-Term Viscosity
K_1, K_2 Glassy Elasticity

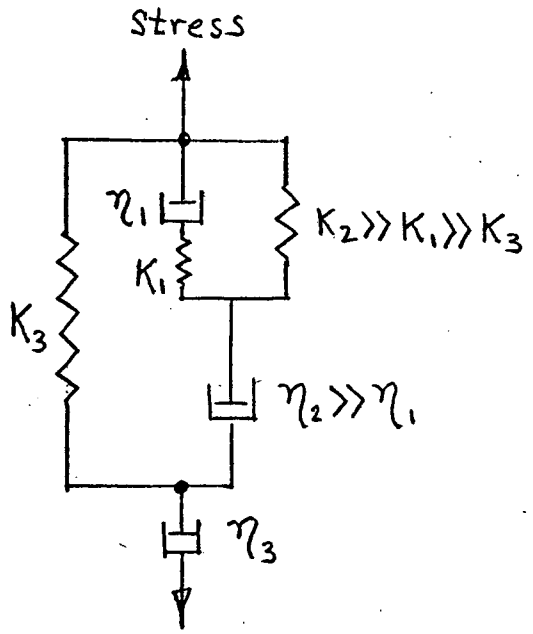

FIG. 3 MECHANICAL ANALOG FOR PHOTOELASTIC MATERIAL

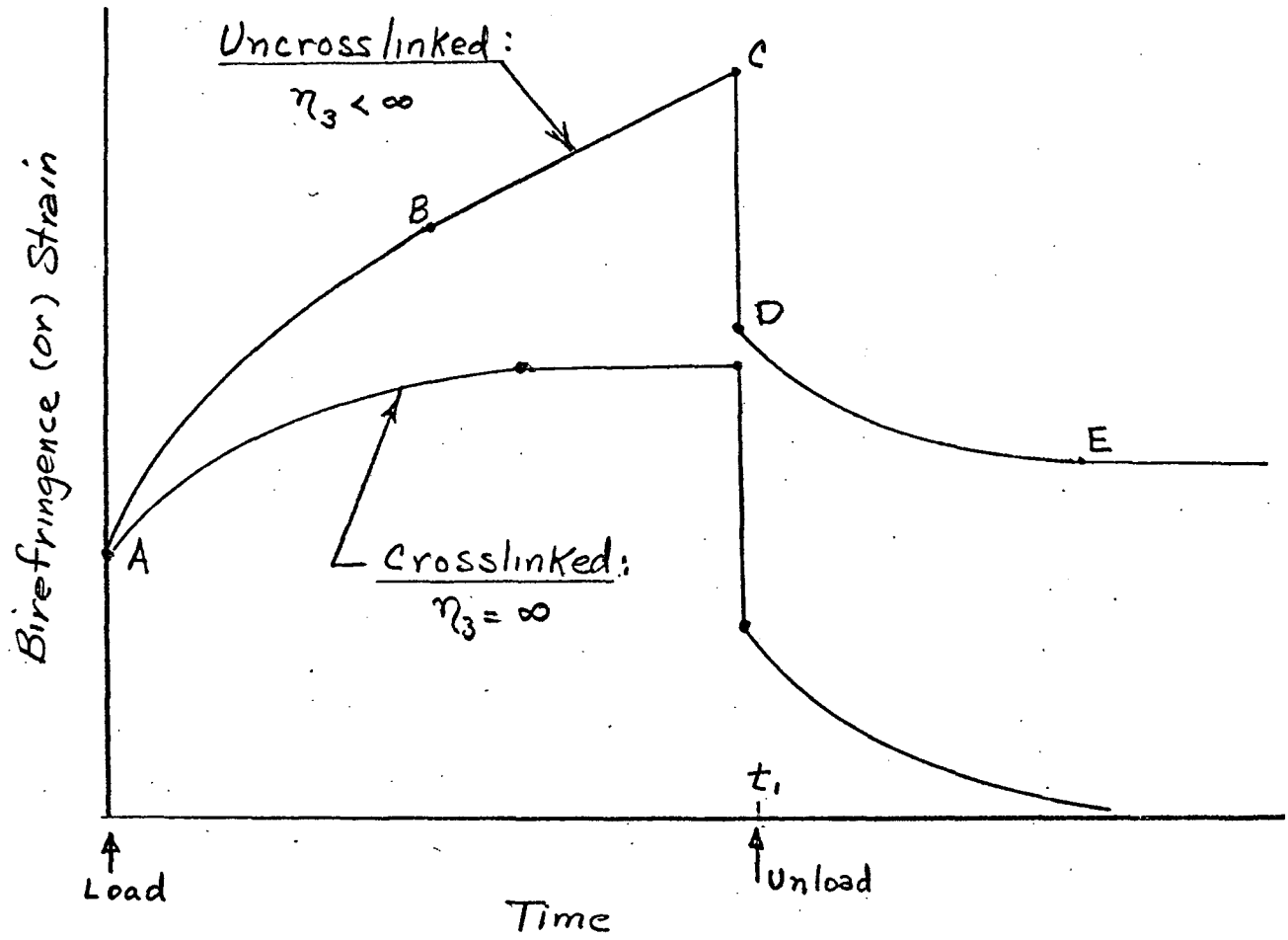

FIG. 4 CHARACTERISTIC BEHAVIOR AT CONSTANT TEMPERATURE

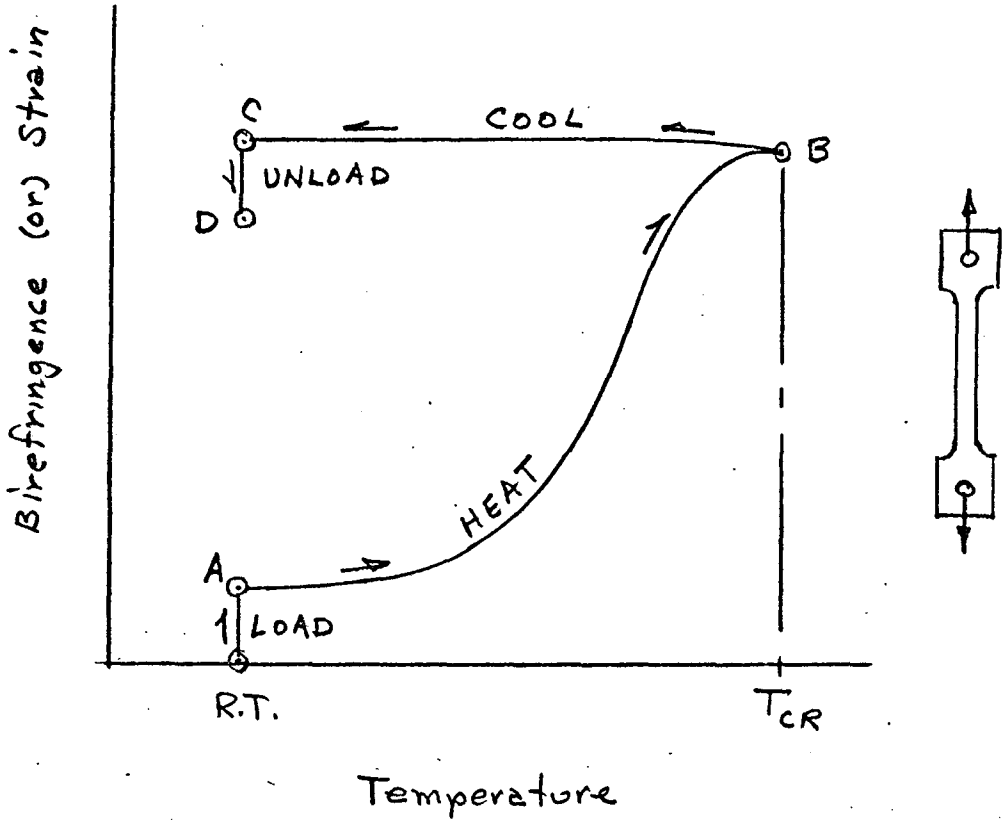

FIG. 5 SCHEMATIC OF "STRESS-FREEZING" PHOTOELASTIC TESTING

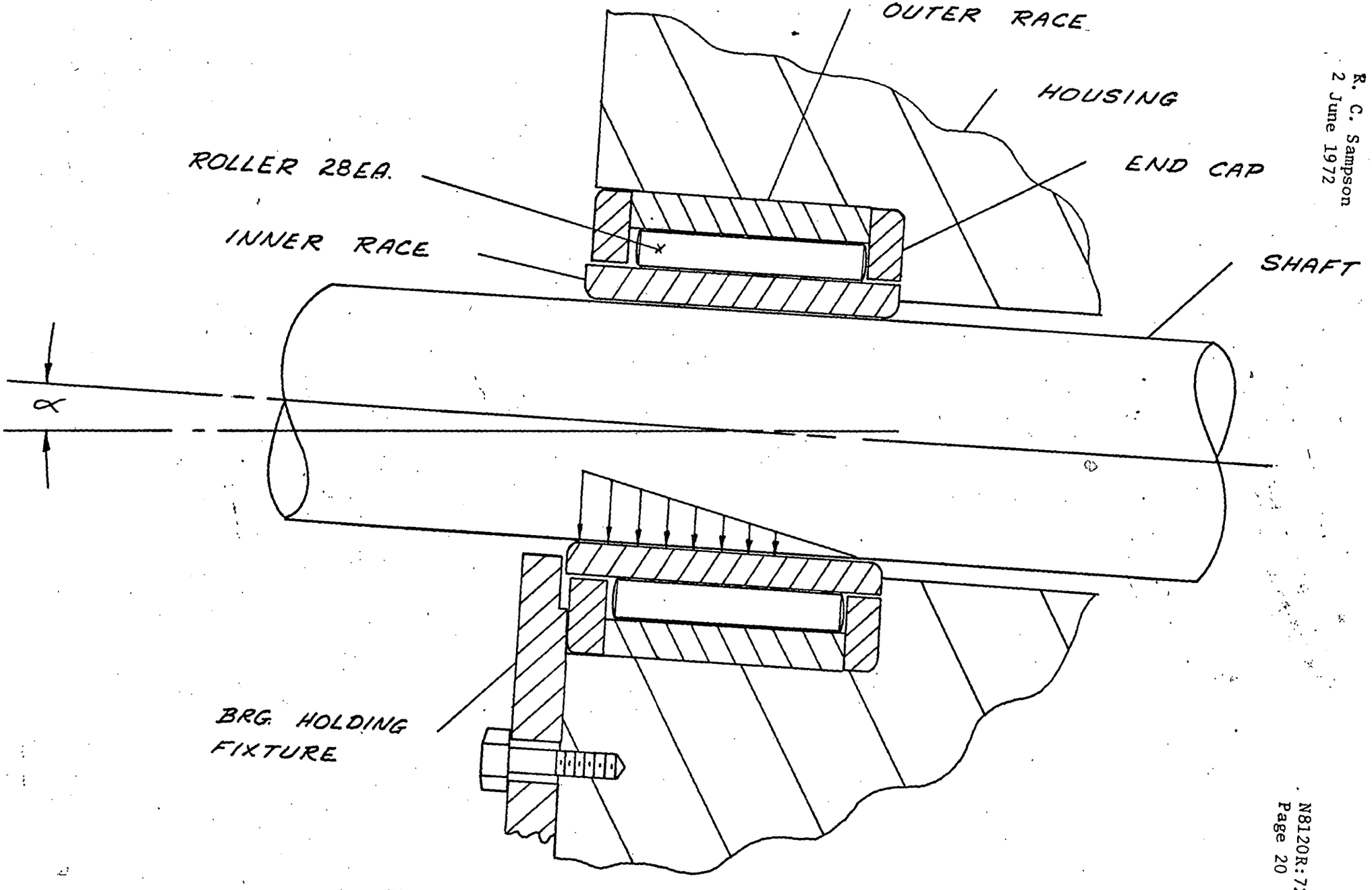

Figure 6 - ROLLER BEARING AND SHAFT MISALIGNMENT

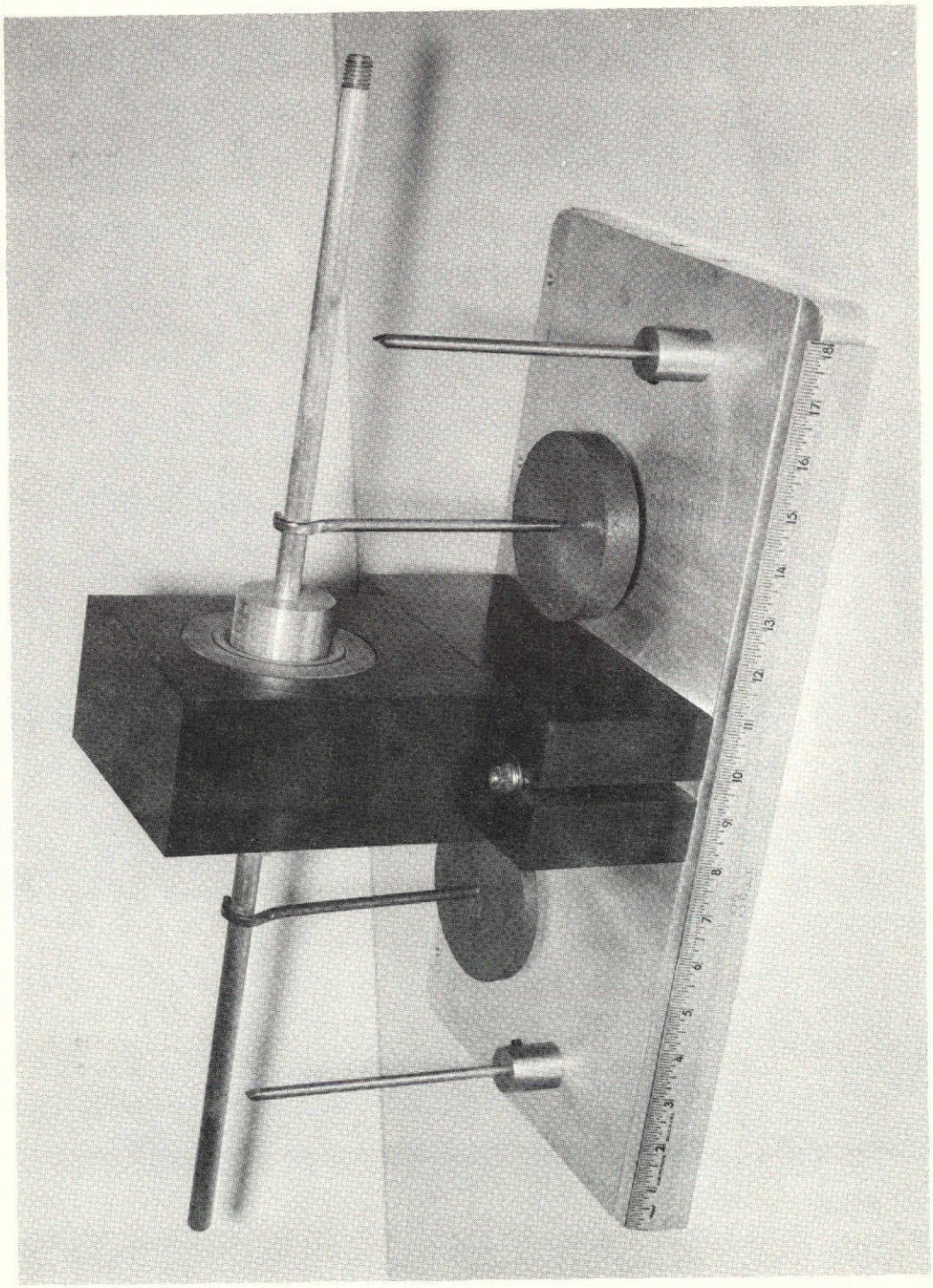

Model with Test Fixtures

Figure 7

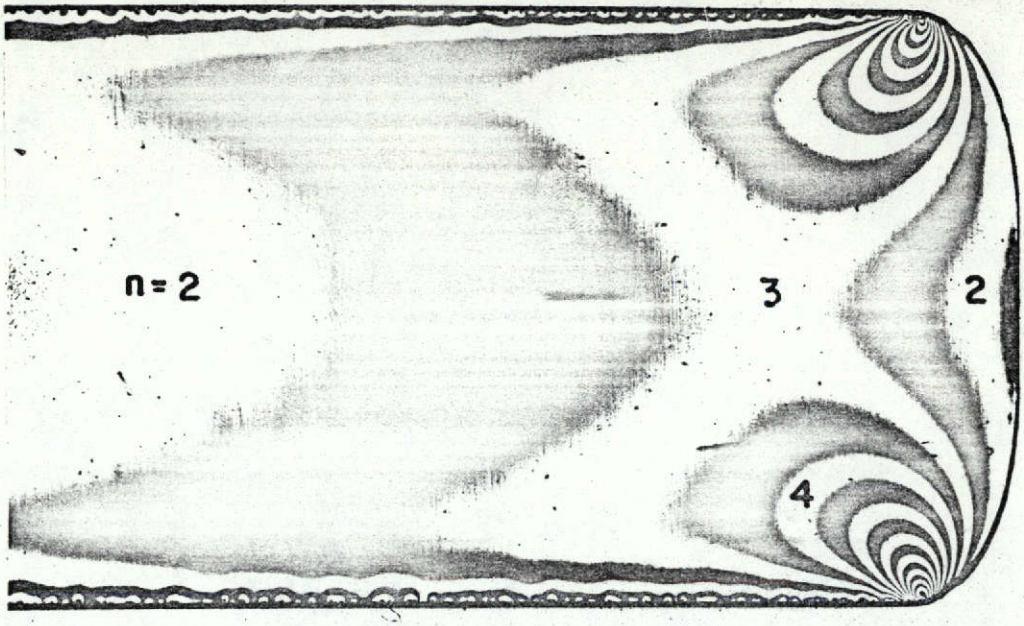

TEST I
(t=.073 in.)

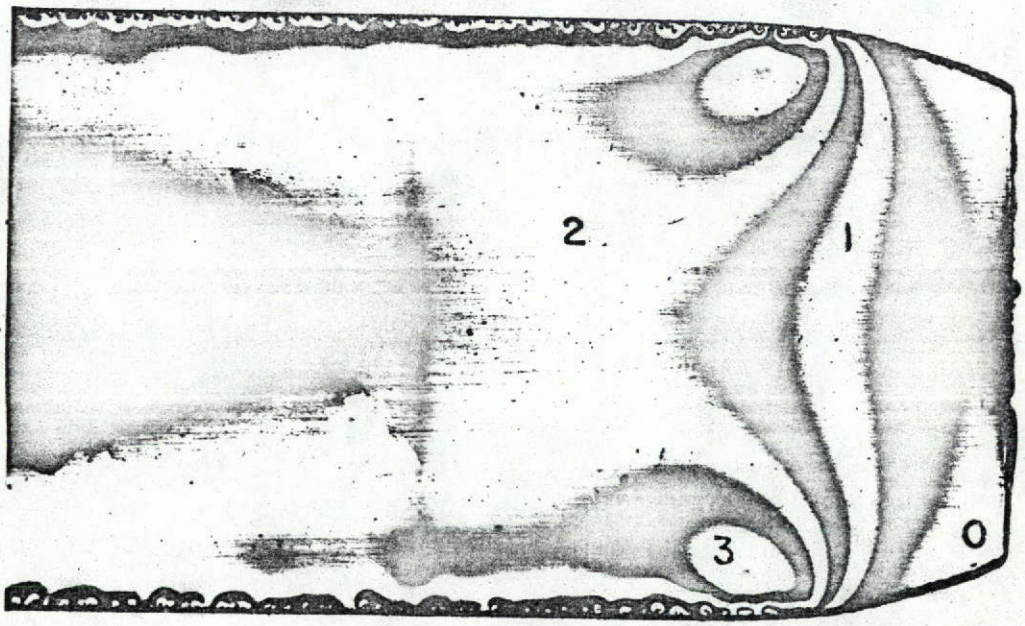

TEST II
(t=.053 in.)

Figure 8 - ROLLER SLICE STRESS PATTERNS

Figure 9 - STRESS DISTRIBUTIONS ON RACE SURFACE, TEST I

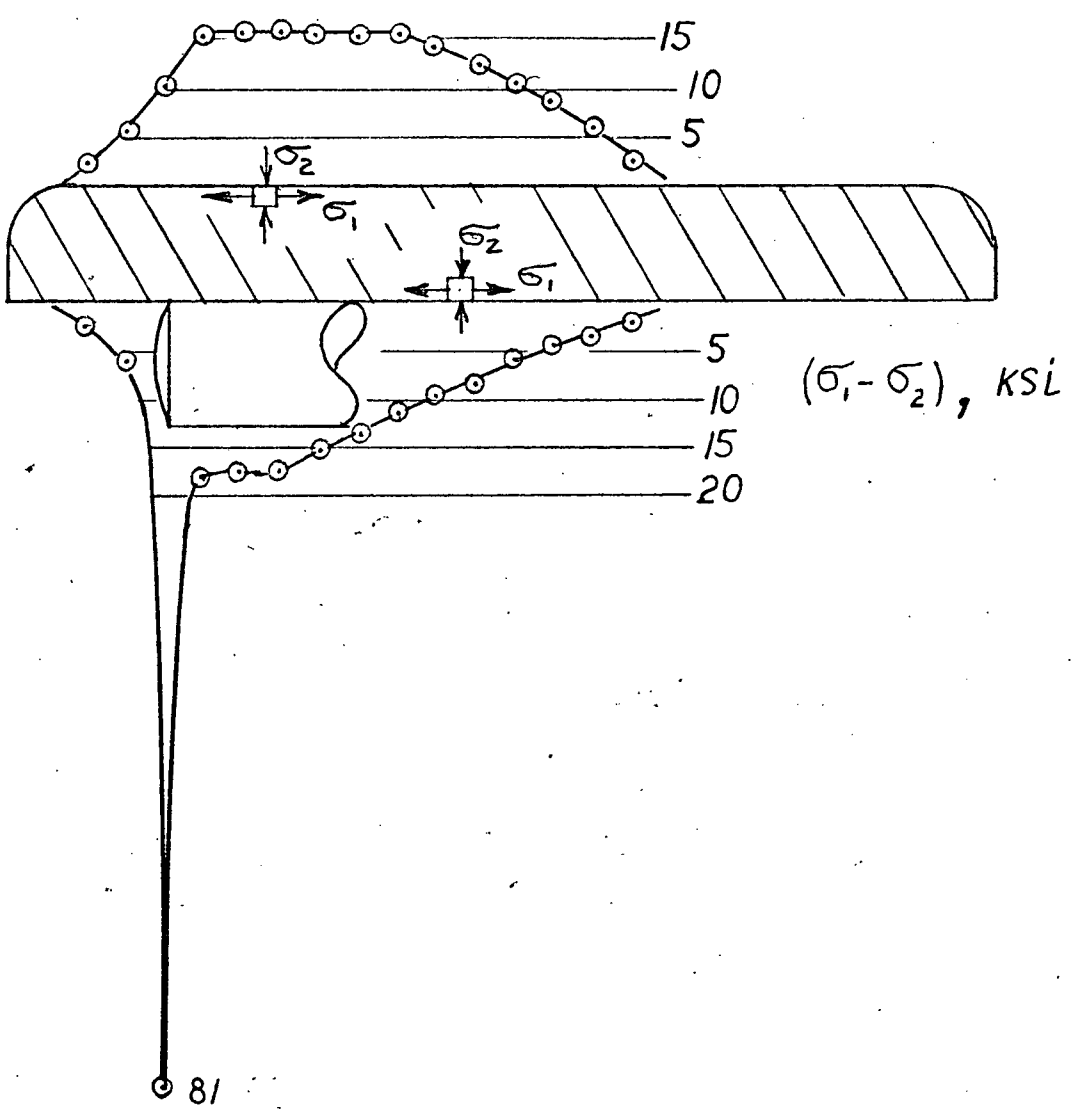

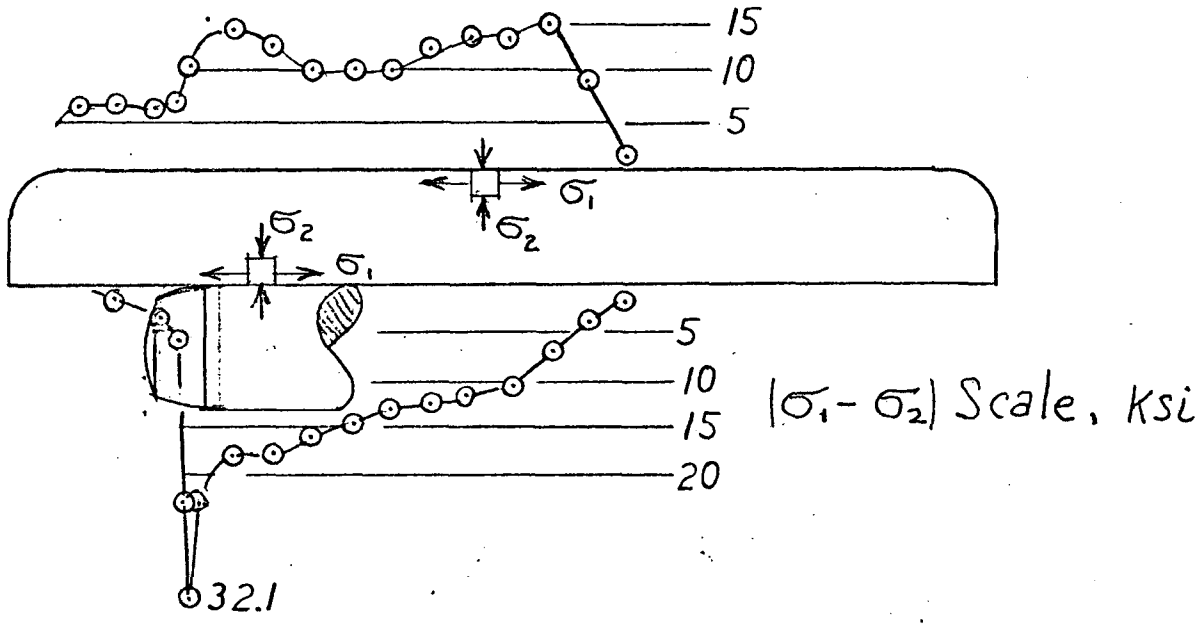

Figure 10 - STRESS DISTRIBUTION ON RACE BOUNDARY, TEST II

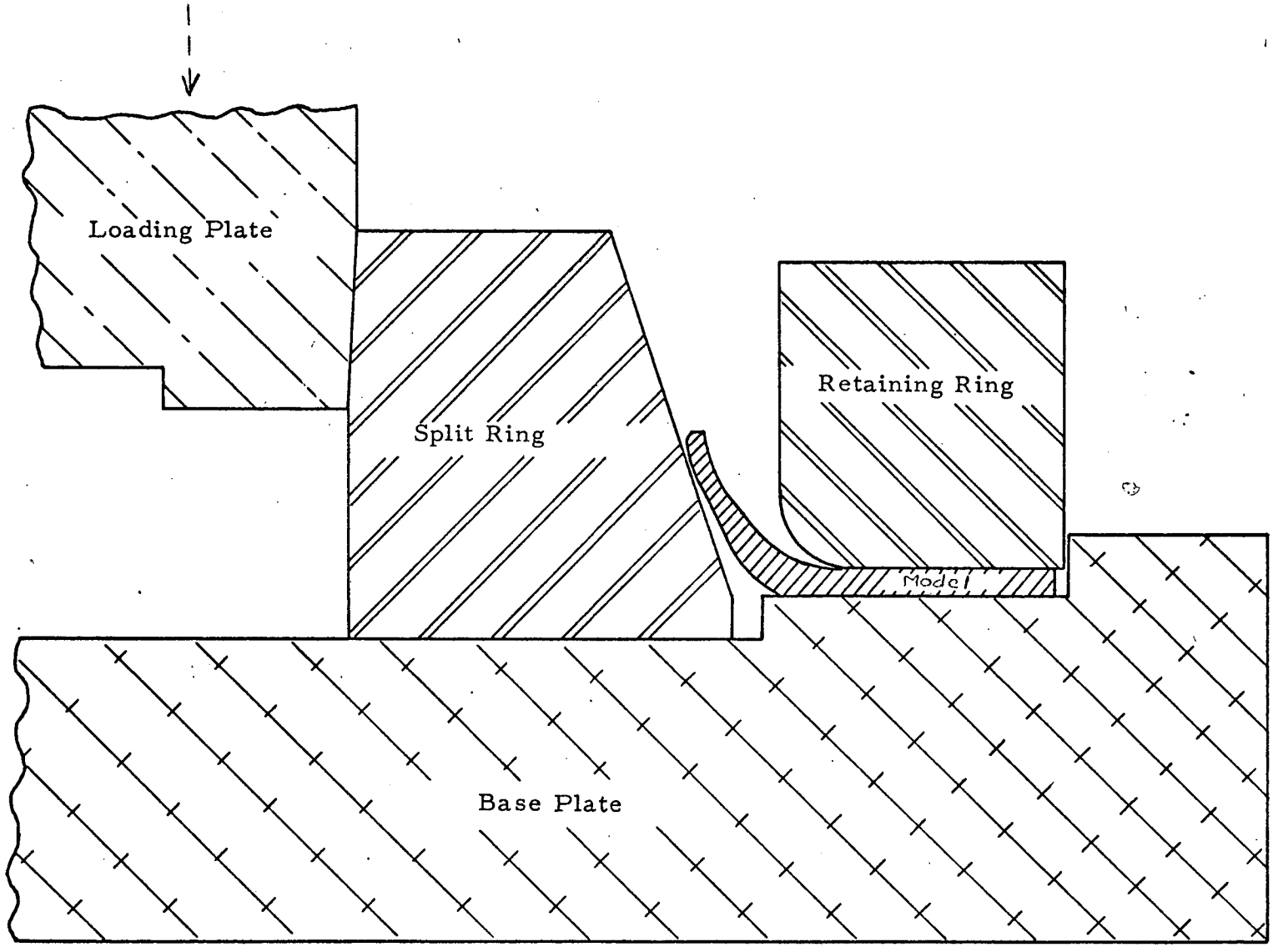

FIGURE 11

DEFLECTION TEST SET-UP

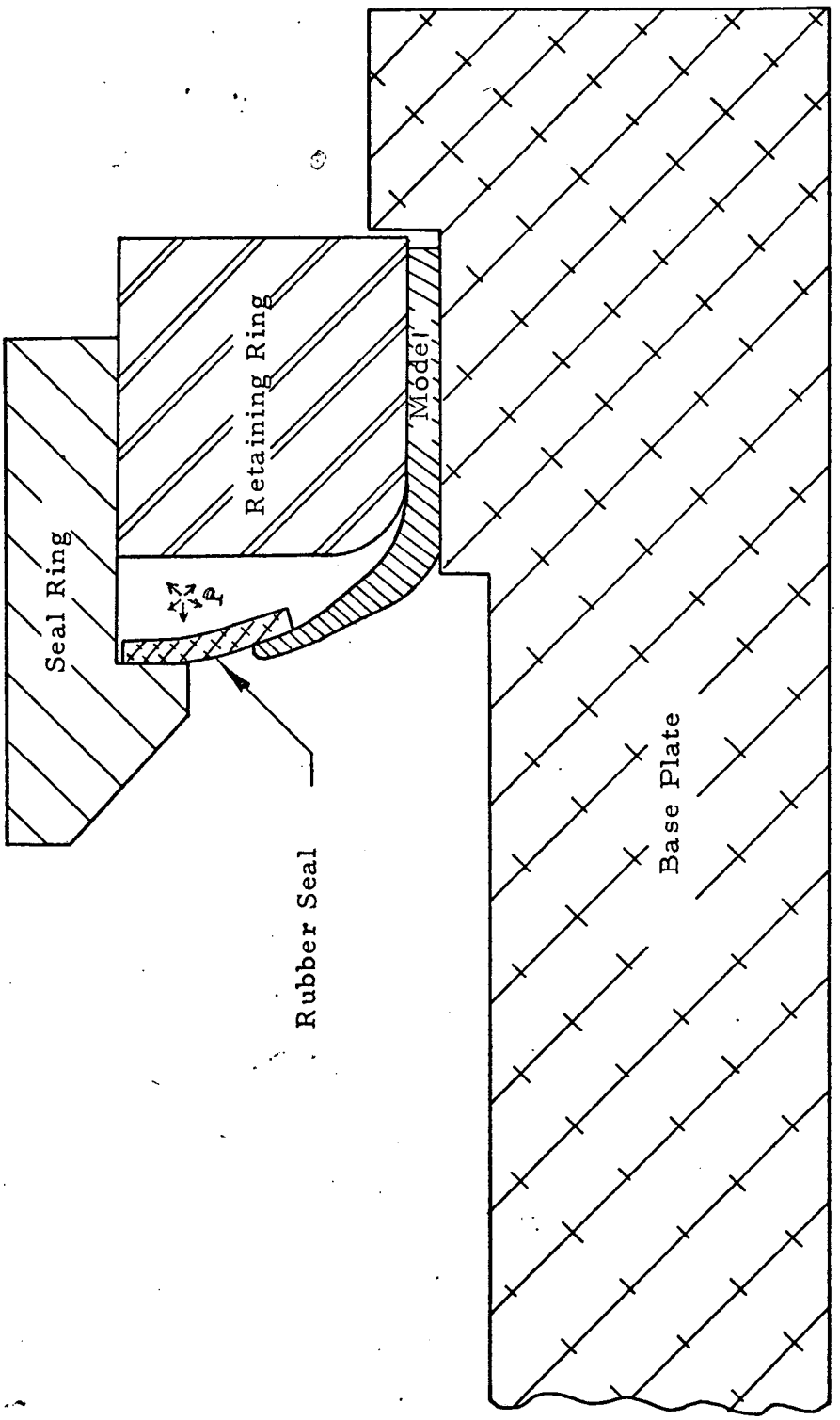

FIGURE 12
PRESSURE TEST SET-UP

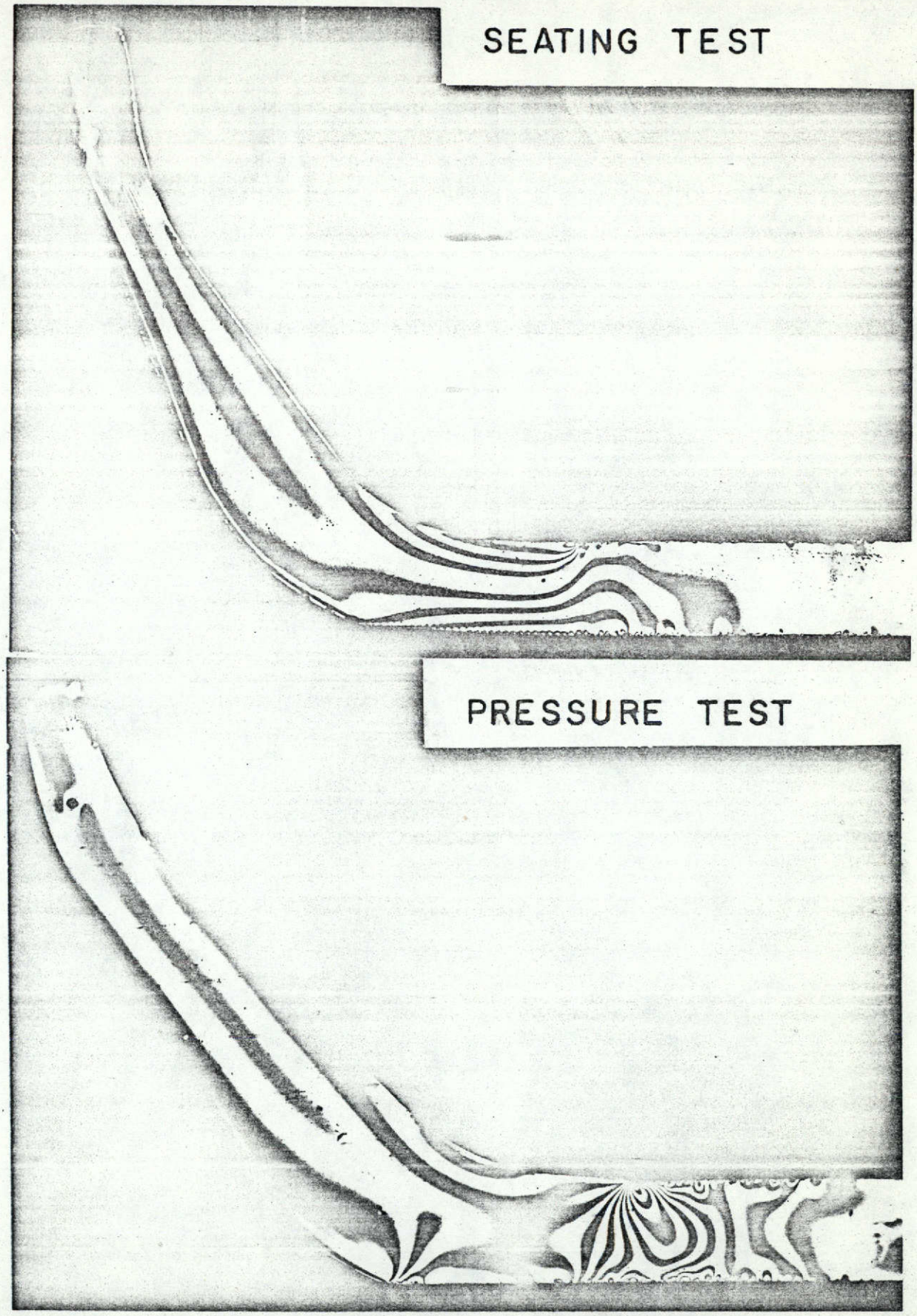

FIG. 13 DARK FIELD FRINGE PATTERNS FROM TYPICAL SLICES OF THE LIP-SEAL MODELS

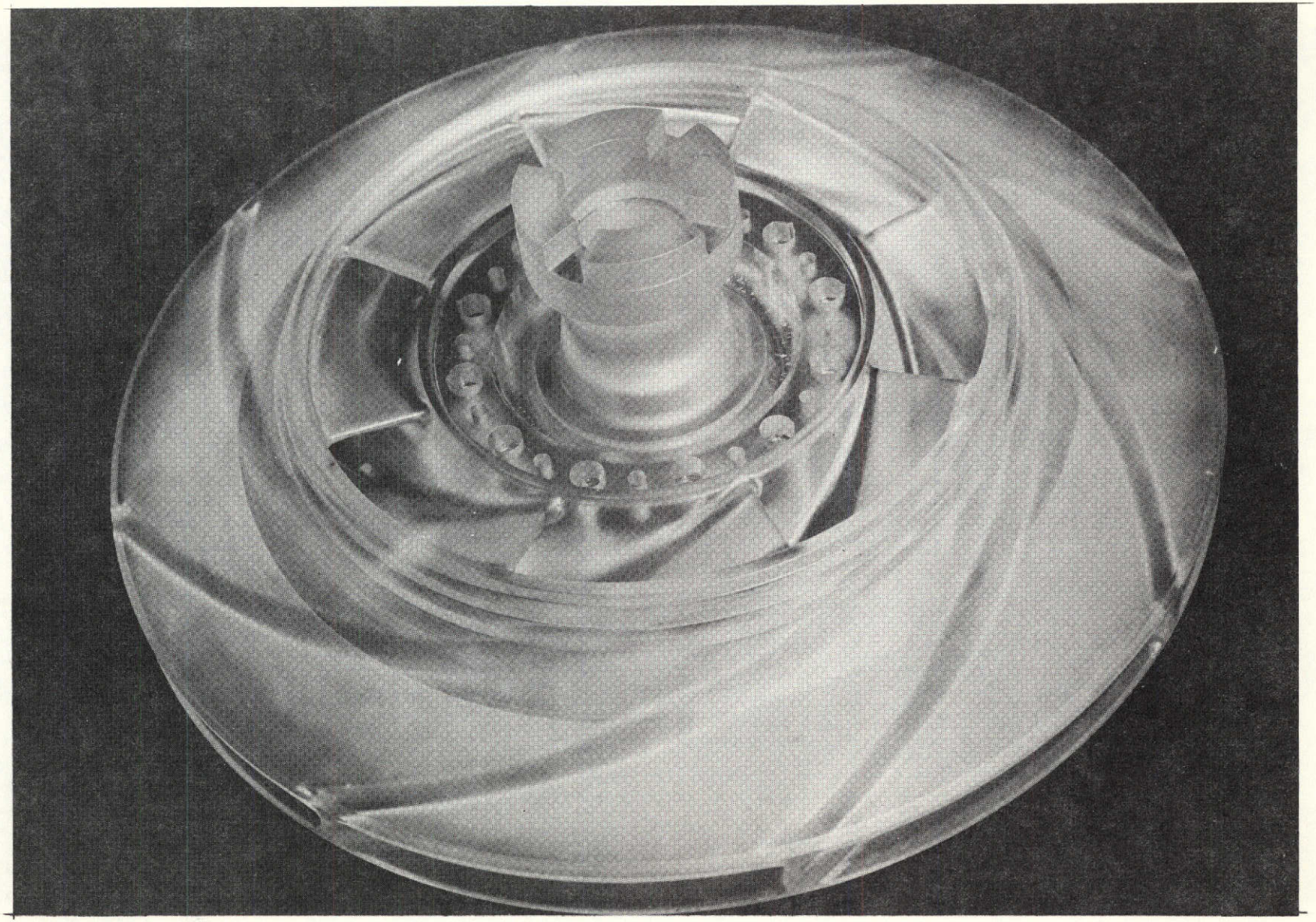

Figure 14 PHOTOELASTIC MODEL IMPELLER

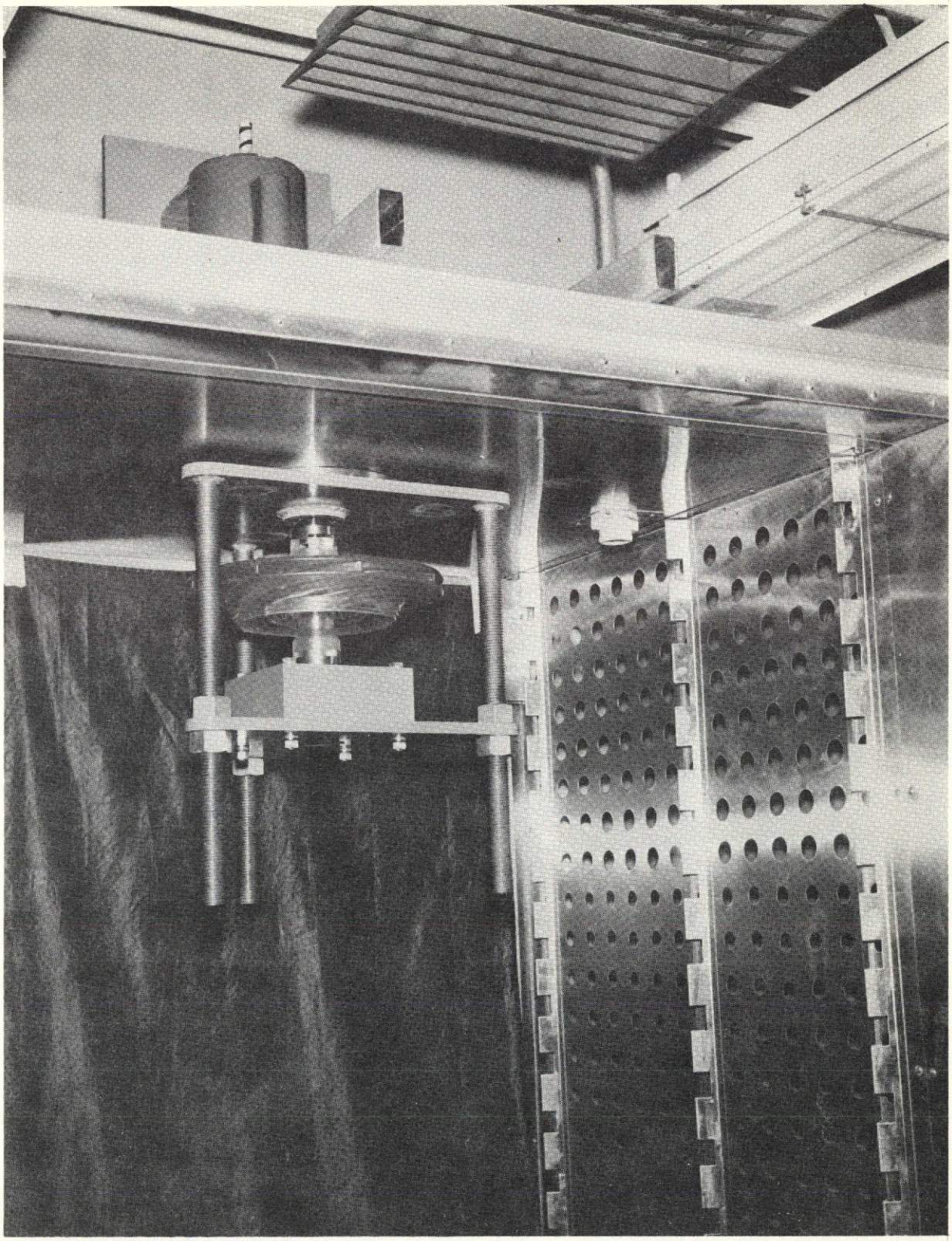

Figure 15. SPIN TEST FIXTURE IN OVEN

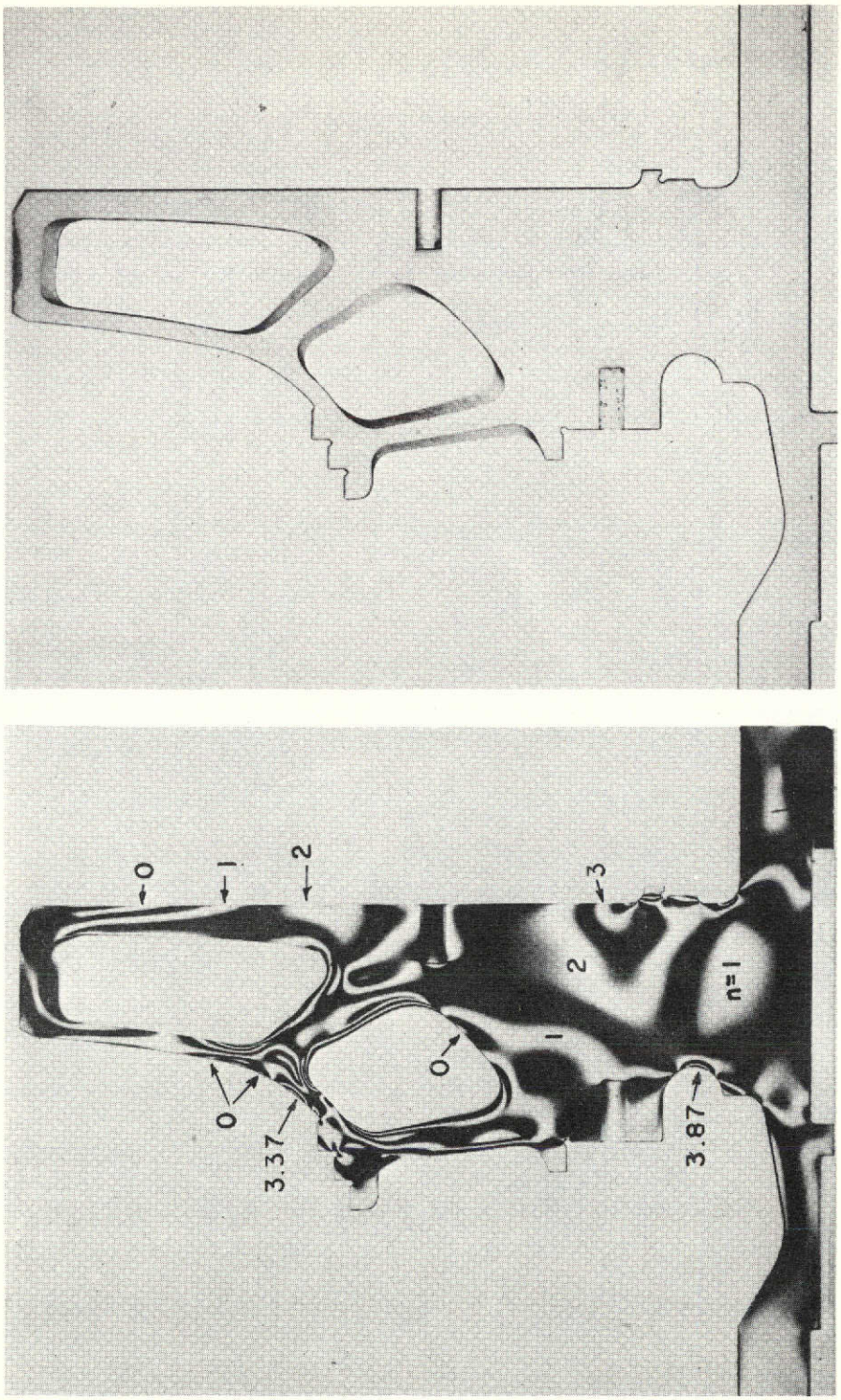

Figure 16 "FROZEN STRESS" PATTERN IN SLICE NO. 1 (Left) AND AFTER ANNEALING (Right)

2:15 p.m. **Discussion**

3:00 p.m. **Tea**

3:30 p.m. *Polymers in Adverse Environments*
R. E. Eshenaur (Manager, Plastics Applications and Evaluations, General Electric Co., Kentucky, U.S.A.)

Chairman: W. F. Watson (Director, Rubber and Plastics Research Association of Great Britain, Shropshire, England)

Panel: N. Grassie (Reader in Chemistry, Glasgow Univ., Scotland)

R. S. Hagan (Manager, Plastics Laboratory, General Electric Co., Kentucky, U.S.A.)

J. B. Howard (Bell Telephone Laboratories, Inc., New Jersey, U.S.A.)

L. N. Phillips (Head of Plastics Technology Section, Royal Aircraft Establishment, Hants., England)

4:00 p.m. **Discussion**

5:00 p.m. **Meeting Adjourns**

TUESDAY, JUNE 17, 1969

9:00 a.m. *High Mechanical Performance—the Engineering Design Problem*
R. M. Ogorkiewicz (Lecturer, Dept. of Mechanical Engineering, Imperial College, London, England)

Chairman: J. H. Crate (Consultant, Plastics Dept., Technical Services Lab., Du Pont Co., Delaware, U.S.A.)

Panel: G. M. Buehrig (Art Center College of Design, California, U.S.A.)

R. A. Horsley (Group Head, Polymer Physics, Shell Research Ltd., Manchester, England)

B. W. Nelson (Dept. Head, Plastics Laboratory, National Cash Register Co., Ohio, U.S.A.)

D. W. Saunders (Prof. of Polymer Physics and Engineering, College of Aeronautics, Cranfield, Bedford, England)

9:30 a.m. **Discussion**

10:15 a.m. **Coffee**

10:45 a.m. *The Problem of Polymer Selection and the Contribution of Plastics to Other Technologies*
A. H. Willbourn (Director of Research, Imperial Chemical Industries Ltd., Plastics Div., Herts., England)

Chairman: F. R. Eirich (Dean of Research, Polytechnic Institute of Brooklyn, New York, U.S.A.)

Panel: L. B. Allen (Manager, Materials Laboratory, International Business Machines, Inc., New York, U.S.A.)

C. E. Hollis (Technical Coordination Manager, BP Plastics Dept., BP Chemicals (UK) Ltd., London, England)

H. J. Sharp (Manager, GKN Plastics Development Centre, London, England)

G. M. Wolf (Manager, Body Materials Engineering Dept., Ford Motor Co., Michigan, U.S.A.)

11:15 a.m. **Discussion**

12:15 p.m. **Lunch**

2:00 p.m. *Processing for High Performance*
J. F. Carley (Assoc. Prof., Dept. of Chemical Engineering, Univ. of Colorado, U.S.A.)

Chairman: M. B. Godfrey (Managing Director, Thermo Plastics Ltd., Bedforshire, England)

Panel: E. Gaspar (Consultant, London, England)

E. C. A. Horner (Polyolefins Technical Service Manager, Imperial Chemical Industries Ltd., Plastics Div., Herts., England)

J. van Leeuwen (Head, Scientific Technical Dept., Plastics and Rubber Research Institute, TNO, Delft, Holland)

I. Rubin (President, Robinson Plastics Corp., New York, U.S.A.)

A. Spaak (Director, Technical Service, Allied Chemical Corp., New Jersey, U.S.A.)

2:30 p.m. **Discussion**

3:15 p.m. **Tea**

3:45 p.m. *New Concepts in Processing*
J. M. Goppel (Koninklijke/Shell Plastics Laboratories, Delft, Netherlands)

Chairman: D. V. Rosato (*Plastics World* magazine, Massachusetts, U.S.A.)

Panel: W. B. Evans (Vice President, Improved Machinery, Inc., New Hampshire, U.S.A.)

A. Kennaway (Consultant, London, England)

G. E. Pickering (Senior Staff Associate, Arthur D. Little, Inc., Massachusetts, U.S.A.)

J. Stafford (Assistant Development Manager, Imperial Chemical Industries Ltd., Plastics Div., Herts., England)

4:15 p.m. **Discussion**

5:00 p.m. **Meeting Adjourns**

Structures Problem-Solving in the Photoelastic Laboratory

Robert C. Sampson, Aerojet-General Corp., Sacramento, Calif.

Photoelasticity is no longer the scientific novelty that formerly evoked expressions of amazement and, oftentimes, over-enthusiasm as to its practical applications. While retaining its unique ability for visual representation of stress in structural models, photoelasticity has matured and found its place due to key advances in materials and techniques. The employment of photoelastic model methods at Aerojet-General Corp. in support of an industrial program for ensuring structural integrity has been highly successful.

In the development of space propulsion systems structural integrity must be maintained, but weight must also be reduced to a minimum. These conflicting requirements pose problems that can be solved in one of three basic ways: (a) build the structure and test it under actual or simulated conditions, (b) analyze the structure by building a mathematical model and testing it in a computer, or (c) fabricate a true scale physical model of the structure and measure its structural performance in closely-controlled laboratory conditions. In practice, methods (a) and (b) provide the major share of the required solutions, but the third alternative can be extremely useful in certain special cases. It is this category of special problems that are described here.

Six examples have been selected from test records to illustrate the variety and scope of the problems that have found most effective treatment by the model techniques. While these examples necessarily reflect a preoccupation with the problems of the rocket motor industry, a similar variety of applications will be found in any industry where strength and weight requirements are in severe conflict, and where there are heavy economic penalties for structural malfunction.

The selected examples illustrate the general areas of utilization: (a) analysis of a complex structure, (b) computer methods verification, (c) materials research, (d) structural design support, and (e) two examples of special technique development to match current problems.

Analysis of a Complex Structure

Problem: A pressurized rocket motor chamber is too complex in shape to analyze the stresses by mathematical methods. How can these stresses be determined?

Solution: Make a true scale model from photoelastic plastics, then "freeze" the stresses by heating and cooling the model while the internal pressure is held constant. Cut thin slices from the model and analyze the frozen stresses in a polariscope.

Example: The intersecting cylinders of the model (*Figure 1*) were cast integral to finish dimensions from an epoxy resin mixture in an acrylic plastic mold.

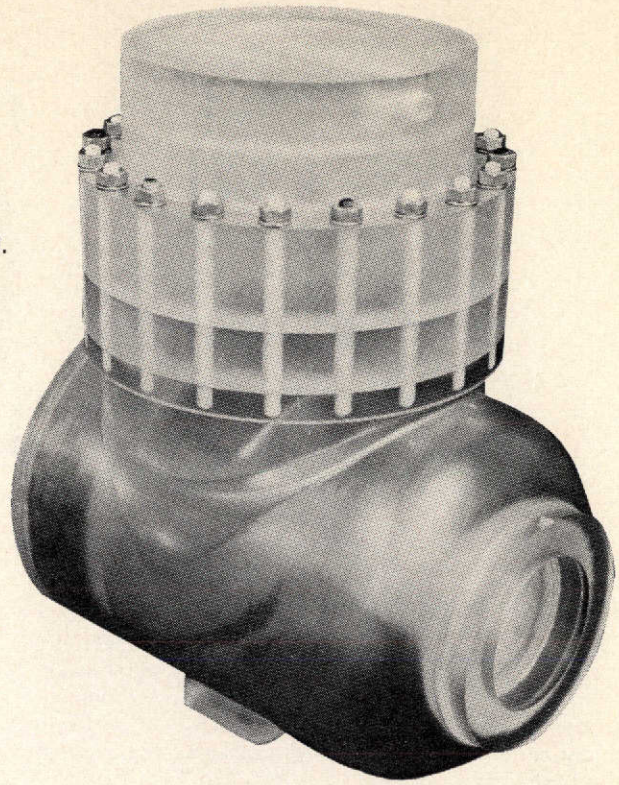

Figure 1. Rocket chamber photoelastic model.

A unique technique is described for visual representation of stresses in structural models

Stresses were frozen under internal fluid pressure (*Test 1, Figure 2*) and fluid pressure combined with a mechanically exerted thrust acting on the flanged top and reacted at the integral pad on the bottom (*Test 2, Figure 2*). The transverse section frozen stress patterns (*Figure 2*) gave all the information needed to accurately depict the surface stress distributions in that plane. The numerical values of fringe order, n, are noted at several locations on *Figure 2*. These values are directly proportional to the stress at each point. Stresses were also determined on a number of other sections, including the line of intersection of the two cylindrical surfaces (*Figure 3*).

Comment: A stress problem too difficult for theoretical analysis was solved by a combination of good model-making technique and the frozen-stress photoelastic method of stress analysis.

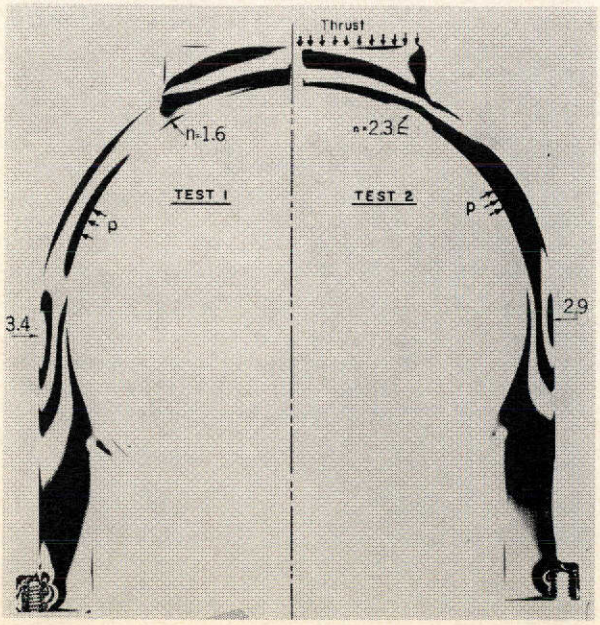

Figure 2. Frozen stress patterns in transverse sections.

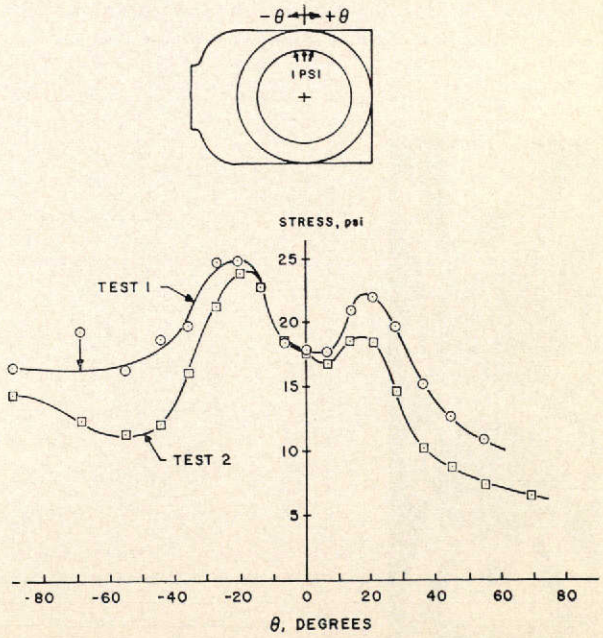

Figure 3. Cylinder intersection stresses.

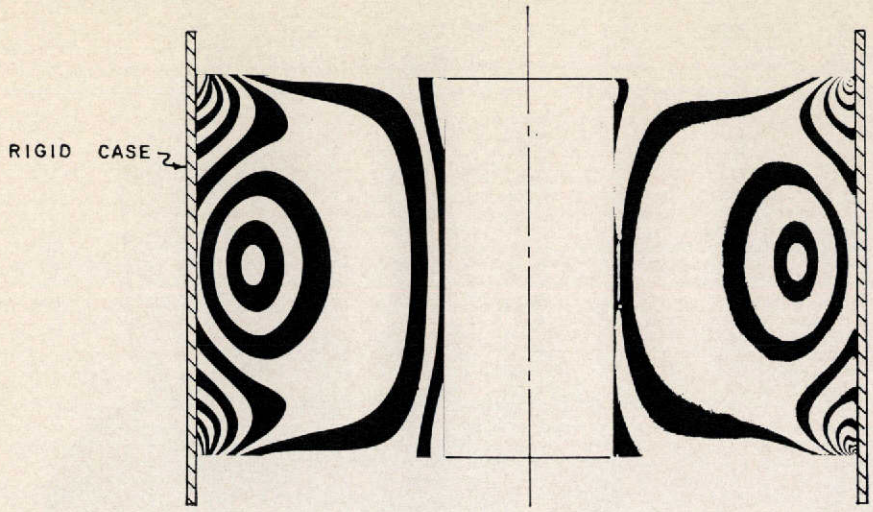

Figure 4. Photoelastic (right) vs computer (left) solution of thermal shrinkage problem in case-bonded grain.

Verifying a Computer Analysis

Problem: Computer solutions of a class of axisymmetric loading problems in case-bonded solid rocket motors had been obtained. It was essential to demonstrate the accuracy of the solution before it was routinely employed in evaluating prototype motor structural integrity.

Solution: Prepare a three-dimensional photoelastic model and freeze the stresses under carefully controlled conditions. Analyze the stress in slices taken from the model and compare the results with the computer stress predictions.

Example: The problem of thermal shrinkage in short, axisymmetric, case-bonded rocket motors had recently provided a numerical solution. Using the experimental technique of the problem on thermal shrinkage in case-bonded propellant grains, a photoelastic solution to this was obtained. The computer data were used to construct a map of half-order birefringence in a meridional plane of the short, case-bonded grain with a concentric circular bore. This artificial stress pattern is shown compared to the real photoelastic pattern in *Figure 4*. It is seen that very good over-all agreement of theory and experiment is indicated. A more explicit comparison was seen in the individual principle stresses along the central radial section, giving excellent quantitative accuracy.

Comment: Confidence in the inherent accuracy of the numerical calculation method was firmly established.

Materials Research Support

Problem: Composite solid propellants consist essentially of rigid particles of oxidizer embedded in a rubbery fuel matrix. Mechanical failure begins at the microstructure level in the binder matrix between rigid particles. Investigate the mechanical aspects of failure initiation between embedded rigid particles.

Solution: Construct superscale photoelastic models of plane sections having rigid disc particles embedded in a soft matrix. Analyze the stresses between adjoining particles and predict the probable failure mechanism. Test these predictions with experiments on arrays of spherical glass beads in a rubbery binder.

Example: Rigid epoxy discs in a matrix of soft photoelastic rubber exhibited stress patterns like that in *Figure 5* (left) when a uniaxial pull was exerted. The nearest neighboring discs, aligned with the load, exert a severe stress concentrated on the binder, as shown by the curves of stress distribution. *Figure 5*

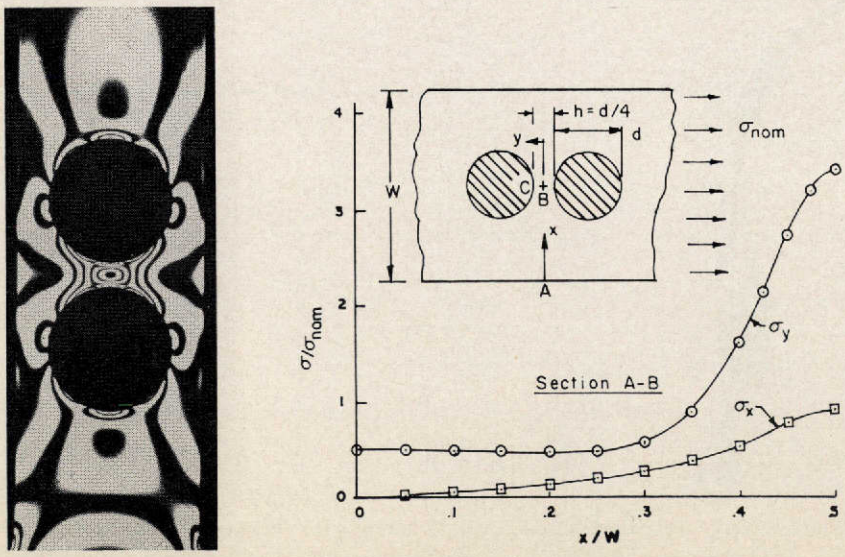

Figure 5. Rigid discs embedded in rubber—photoelastic pattern (left) and stress distributions (right).

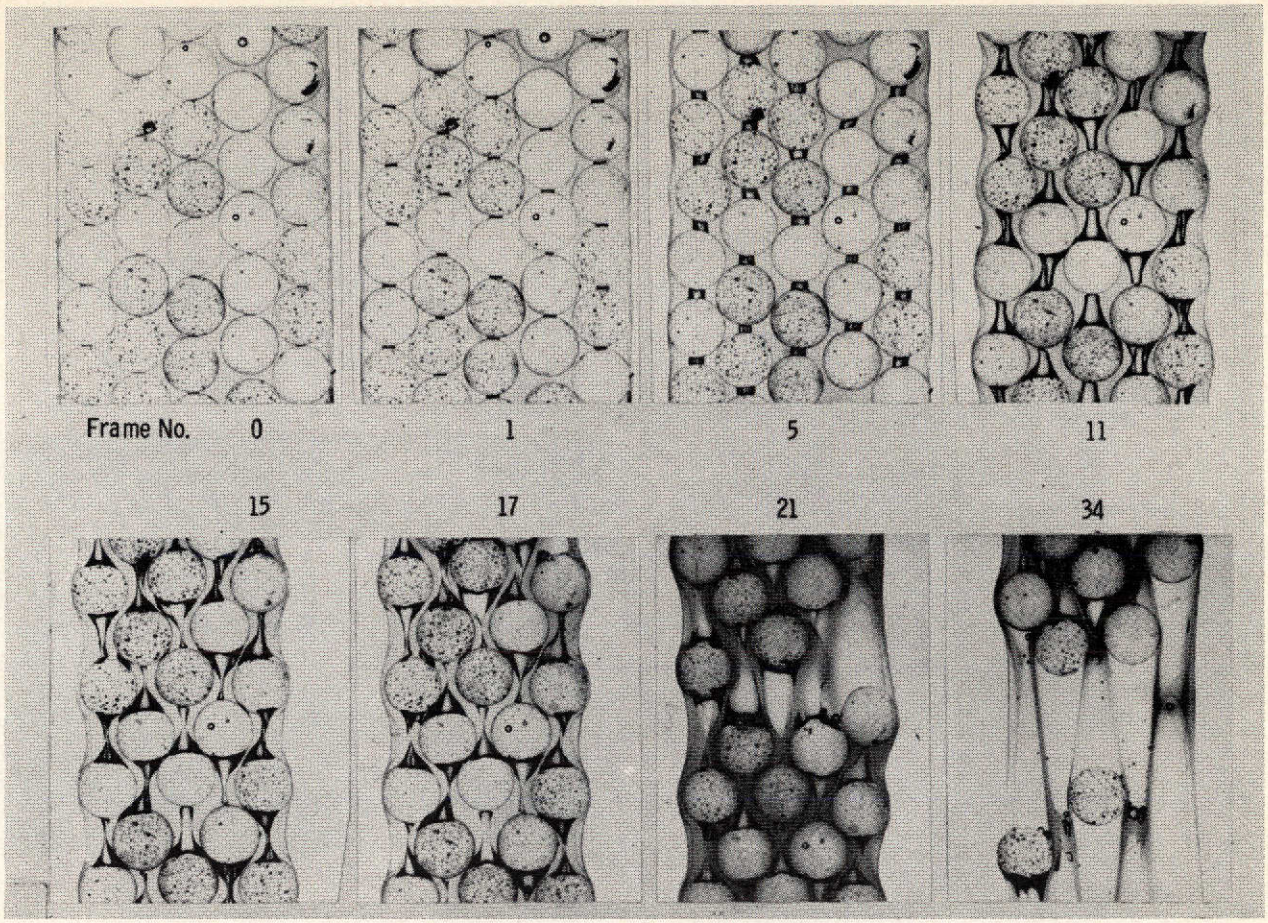

Figure 6. Progressive damage in a composite model.

(right). Failure may equally likely initiate at the disc/binder interface bond or in the interior of the binder ligament. These conclusions were tested by observing the failure behavior of 5 x 9 arrays of glass balls embedded in a soft rubber binder. Sequence photographs from one such test (*Figure 6*) show early initiation of cohesive failures between neighboring beads aligned with the load, Frame 1. Marked changes of the stress-strain characteristic were noted near Frames 5 and 17, and a local weakness leading to eventual failure is evident in Frame 21. Similar experiments with different binders showed how the structural performance of the composite is most strongly affected by the binder properties, and that different failure processes result from different binder properties.

Comment: Superscale model techniques are often very useful in delineating the mechanical principles of behavior in microscopic composites. Insights are gained that might be obscured in "real" composites.

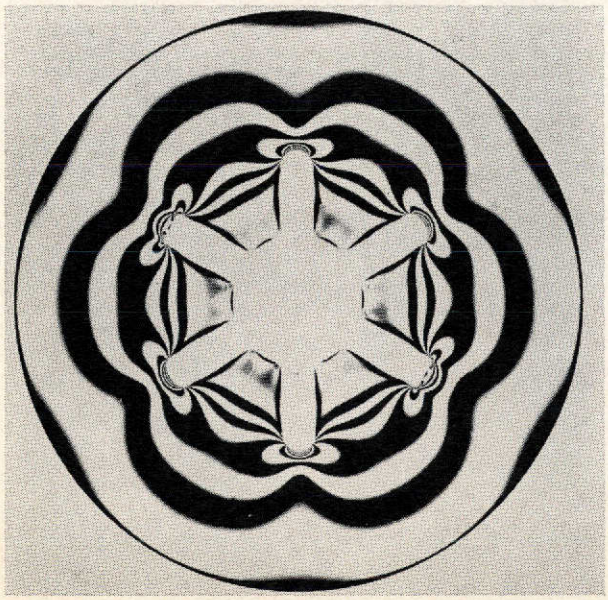

Figure 7. Photoelastic test specimen of a propellant grain.

Stress Data in Support of Structures Design

Problem: Grain design engineers must often weigh the effects of grain geometry changes on both the stress and combustion efficiency of the design. Design data are needed that relates the stress concentration at the "star points" of a grain cross section to its geometric parameters.

Solution: Design, build and test a series of two-dimensional photoelastic models that encompass a wide range of the important geometric parameters. Expand the useful scope of the test data by cross-plotting and interpolating.

Example: A typical 2-D model is shown in *Figure 7*. The frozen stress pattern was induced by the thermal shrinkage stress-freezing process described in the problem of thermal shrinkage in case-bonded propellant grains. Stress concentration data (maximum fillet

stress per unit external pressure) obtained from a series of models of this type are shown in *Figure 8*. These curves allow the designer to assess the consequences of a wide variety of geometric changes, with good engineering accuracy.

Comment: In plane structures with few shape parameters, extensive design data can often be obtained at moderate cost.

Propellant Strain Measurement Technique Development

Problem: The behavior of solid propellants in the presence of high strain concentrations is not readily predicted. Develop a convenient means for measuring surface strain distributions on actual propellant specimens.

Solution: The moirè grid-interference method was adapted to this purpose. Investigation showed that the most effective approach utilized a grid pattern printed on the surface of the test specimen. Grid photographs of the loaded specimen, obtained at 1:1 magnification, contain all the information needed to determine the surface strain distribution. A novel "grid-shift" technique was developed to speed the accurate analysis of the moirè fringe data.

Example: A slotted, wedge-shaped propellant test specimen closely represents the stress concentration in a solid rocket grain. A specimen of this kind with printed surface grids of 100 lines/in. was photographed, and quantitative analysis of the moirè grid photographs (*Figure 9*) showed that the strain concentration factor increased repidly as failure at the notch was approached.

Comment: Moirè methods allow detailed strain analysis on real solid propellant materials tested in realistic environmental conditions.

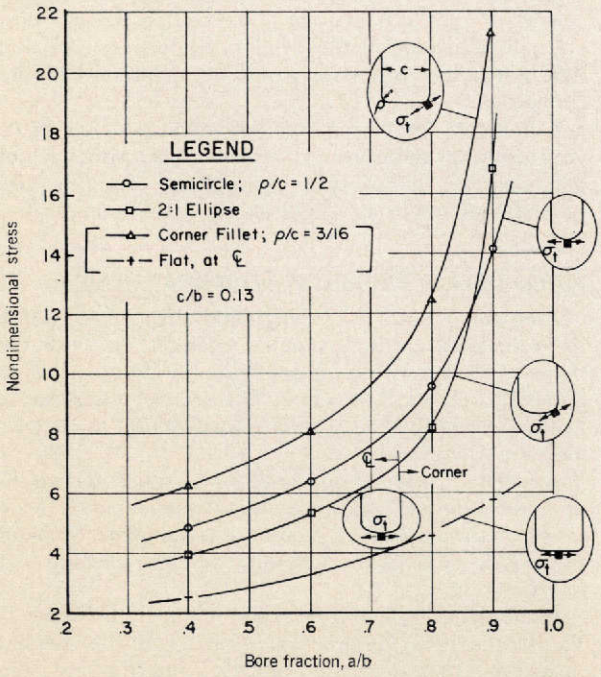

Figure 8. Effect of slot-end configuration on maximum fillet stress.

Thermal Shrinkage in Case-Bonded Propellant Grains

Problem: Solid propellants expand and contract with temperature approximately ten times more than the rigid outer case materials, and severe interaction between the case and the grain is encountered. How can these stresses and strains be evaluated for complex three-dimensional motors? Conventional stress-freezing photoelastic methods are not suitable for this class of problem.

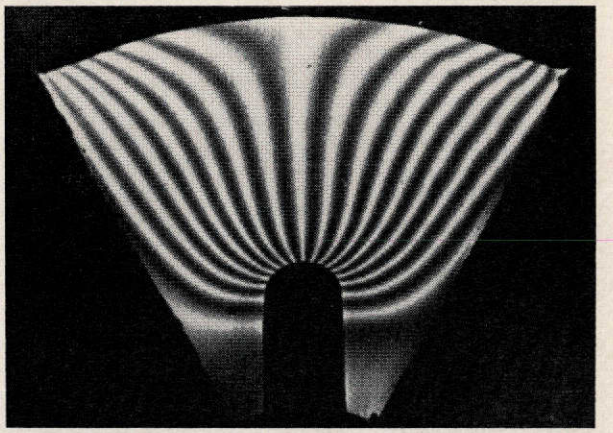

Figure 9. Moire displacement fringe pattern in propellant test sample.

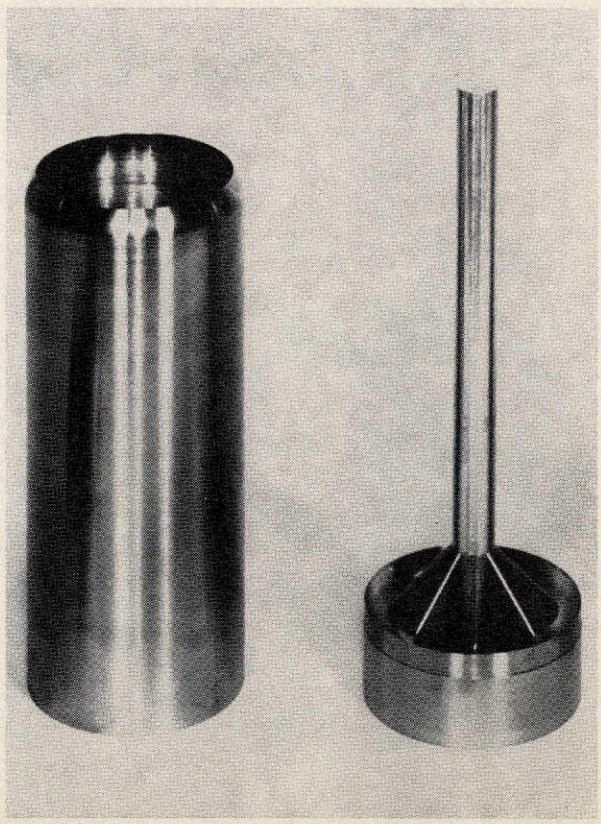

Figure 10. Casting mold and finned cylindrical core for 3-D grain model.

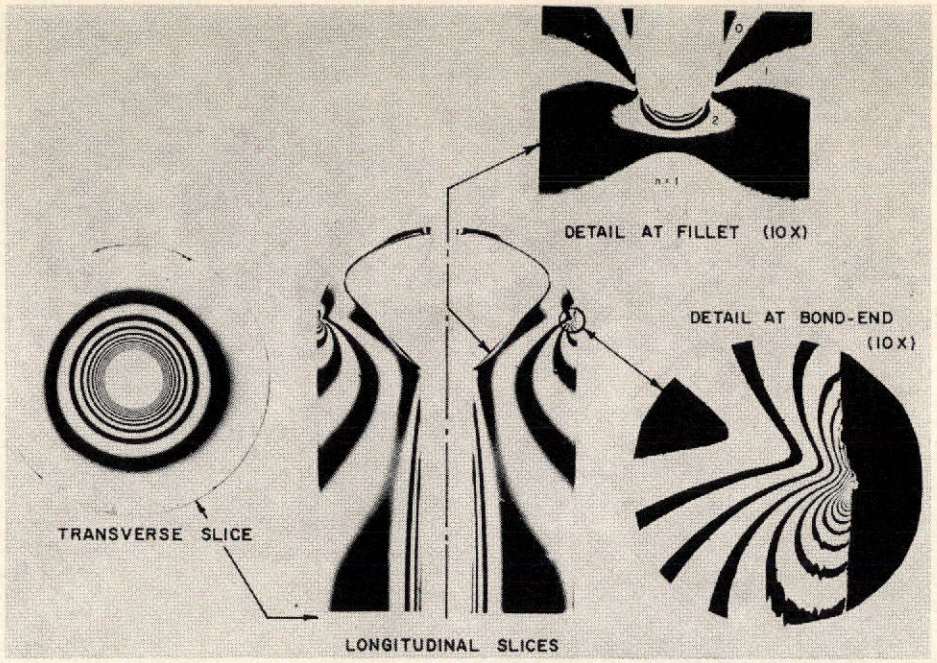

Figure 11. Frozen stress slices from 3-D grain model thermal shrinkage test.

Solution: A novel stress-freezing technique was developed to permit photoelastic simulation of propellant shrinkage conditions. In this method, a true-scale model is cast to shape in liquid epoxy resin and cured at gradually elevated temperature while bonded to the subscale model case. Cooling the composite model structure induces the same stress condition experienced by the motor. Differential shrinkage stress is frozen in and is accurately resolved in a quantitative manner, using special model materials and calibration techniques.

Example: The subscale metal case and cores are shown in *Figure 10*. The large fins attached at the forward end of the cylindrical aluminum core are made from Wood's metal to facilitate easy removal after solidification of the cast liquid resin. After the stress-freezing cycle is completed, the metal case is slit and peeled away. Thin slices taken at various sections and viewed in polarized light (*Figure 11*) give all the information needed for detailed stress determinations.

Comment: Differential contraction in very complex composite structures was made amenable to experimental model analysis by devising a new, three-dimensional stress-freezing technique. This type of problem has widespread significance in solid propellant rocket motor structural integrity.

Conclusion

These representative examples illustrate that the photoelastic laboratory is far removed from being a routine testing facility. On the contrary, the ability to modify existing techniques or devise new ones to cope with non-routine problems is readily seen to be its most valued asset. Maintaining and improving this capability is one of the laboratory's primary functions. Consequently, the laboratory maintains a steady research effort aimed at improving model materials, experimental techniques and instrumentation. Only in that way can a suitable repertoire of techniques be made ready for the new problems that periodically appear in an advancing industry.

References

1. Handbook of Experimental Stress Analysis, M. Hetenyi, ed., John Wiley & Sons, New York, N. Y.
2. Leven, M. M. and Sampson, R. C., "Photoelastic Stress and Deformation Analysis of Nuclear Reactor Components," Proceedings of the SESA, Vol. XVII, no. 1, 1959.
3. Sciammarella, C. A. and Durelli, A. J., "Moirè Fringes as a Means of Analyzing Strains," *Journal of Engineering Mechanics*, Proceedings of the ASCE, Vol. 8, EM 1, February 1961.
4. Sampson, R. C. and Campbell, D. M., "The Grid-Shift Technique for Moirè Analysis of Strain in Solid Propellants," *Experimental Mechanics*, Vol. 7, no. 11, November 1967.
5. Sampson, R. C., "A Three-Dimensional Photoelastic-Method for Analysis of Differential Contraction Stresses," *Experimental Mechanics*, Vol. 3, no. 10, October 1963.

About the Author

Robert C. Sampson received his BS in mechanical engineering in 1947 at the University of Washington. He was first employed in the Westinghouse Electric Corp. student training program, and later spent three years in analysis of aircraft gas turbine structures. Subsequently he transferred to the Westinghouse Research Laboratories where he was a research engineer in photoelastic stress analysis. Joining the Aerojet-General Corp. in 1960, Mr. Sampson has directed the activities of the photomechanics laboratory at the firm's Sacramento plant since that time.

It's an Impco! The machine that really hustles.
On short runs. On long runs. On any run. While you take it easy.
Because for one thing, you have the benefit
of the most advanced automatic design in the field.
For another, it's loaded with Impco standard features.
And with an Impco, there's just *one source of*
sales and service responsibility.

IMPCO®

A subsidiary of Ingersoll-Rand

Improved Machinery Inc., Nashua, N.H., Canada: Impco Plastic Machinery, Ltd., Great Britain: Ingersoll-Rand Co., Ltd., London, Europe: Sunds AB, Oerebro, Sweden